

Discovering a misaligned CO outflow related to the red MSX source G034.5964-01.0292

S. Paron^{1,2}, M. E. Ortega¹, A. Petriella¹, and M. Rubio³

¹ Instituto de Astronomía y Física del Espacio (IAFE), CC 67, Suc. 28, 1428 Buenos Aires, Argentina
 e-mail: sparon@iafe.uba.ar

² FADU and CBC – Universidad de Buenos Aires, Ciudad Universitaria, 1428 Buenos Aires, Argentina

³ Departamento de Astronomía, Universidad de Chile, Casilla 36-D Santiago, Chile

Received 21 February 2014 / Accepted 10 June 2014

ABSTRACT

Aims. The red MSX source G034.5964-01.0292 (MSXG34), catalogued as a massive young stellar object, was observed in molecular lines with the aim of discovering and studying molecular outflows.

Methods. We mapped a region of $3' \times 3'$ centred at MSXG34 using the Atacama Submillimeter Telescope Experiment in the $^{12}\text{CO } J = 3-2$ and $\text{HCO}^+ J = 4-3$ lines with an angular and spectral resolution of $22''$ and 0.11 km s^{-1} . Additionally, public $^{13}\text{CO } J = 1-0$ and near-IR UKIDSS data obtained from the Galactic Ring Survey and the WFCAM Science Archive were analysed.

Results. We found that the ^{12}CO spectra towards the YSO present a self-absorption dip, as is common in star-forming regions, and spectral wings that indicate outflow activity. The HCO^+ was detected only towards the MSXG34 position at $v_{\text{LSR}} \sim 14.2 \text{ km s}^{-1}$, in coincidence with the ^{12}CO absorption dip and approximately with the velocity of previous ammonia observations. HCO^+ and NH_3 are known to be enhanced in molecular outflows. When we analysed the spectral wings of the ^{12}CO line, we discovered misaligned red- and blue-shifted molecular outflows associated with MSXG34. The near-IR emission shows a cone-like nebulosity composed of two arc-like features related to the YSO, which might be due to a cavity cleared in the circumstellar material by a precessing jet. This can explain the misalignment in the molecular outflows. From the analysis of the $^{13}\text{CO } J = 1-0$ data we suggest that the YSO is very likely related to a molecular clump ranging between 10 and 14 km s^{-1} . This suggests that MSXG34, with an associated central velocity of about 14 km s^{-1} , may be located in the background of this clump. Thus, the blue-shifted outflow is probably deflected by the interaction with dense gas along the line of sight. From a spectral energy distribution analysis of MSXG34 we found that its central object probably is an intermediate-mass protostar.

Key words. stars: formation – ISM: jets and outflows – ISM: molecules

1. Introduction

One of the most remarkable and not yet completely understood processes involved in the formation of stars is the appearance of collimated bipolar outflows in the earliest stages of formation. This process is present until the end of the accretion phase and has significant effects in the surroundings (e.g. [Froebrich et al. 2003a,b](#); [Bally et al. 2006](#); [Arce et al. 2010](#)). The structure and (a)symmetries of the outflows record orientation changes of the accretion disk and motion of the source relative to the local interstellar medium ([Cunningham et al. 2009](#)). Moreover, the outflows can be deflected by material swept up in an earlier epoch of ejection by the central source ([Fich & Lada 1997](#)) and/or by dense preexisting molecular clumps ([Choi 2005](#); [Baek et al. 2009](#)). Thus, mapping molecular outflows is very useful for studying star formation, and in particular, for investigating the interaction between young stellar objects (YSOs) and the surrounding environments.

The red MSX source G034.5964-01.0292 (hereafter MSXG34), related to IRAS 1855+0056, is catalogued as a massive YSO located at a distance of 1.1 kpc ([Lumsden et al. 2013](#)). Ammonia was detected towards this source by [Wienen et al. \(2012\)](#). The $(J, K) = (1, 1)$ and $(2, 2)$ NH_3 inversion lines were detected at velocities of 13.63 and 13.84 km s^{-1} , related to the ATLASGAL source G34.60-1.03 detected at $870 \mu\text{m}$. This source lies at the north-eastern border of the HII region G34.5-1.1, that has a recombination line

at 44.7 km s^{-1} ([Lockman 1989](#); [Kuchar & Clark 1997](#)); this precludes any connection between them. Thus, taking into account that very likely a massive YSO is related to dense material traced by the ammonia emission, and that no others YSOs are catalogued around this source, which would make an outflow study confusing, we decided to observe MSXG34 in the $^{12}\text{CO } J = 3-2$ and $\text{HCO}^+ J = 4-3$ lines to search for signatures of molecular outflows.

2. Observations and data reduction

The molecular observations presented in this work were carried out on September 13, 2013 with the 10 m Atacama Submillimeter Telescope Experiment (ASTE; [Ezawa et al. 2004](#)). We used the CATS345 receiver, which is a two single-band SIS receiver remotely tunable in the LO frequency range of 324–372 GHz. We simultaneously observed $^{12}\text{CO } J = 3-2$ at 345.796 GHz and $\text{HCO}^+ J = 4-3$ at 356.734 GHz, mapping a region of $3' \times 3'$ centred at $\text{RA} = 18^{\text{h}}58^{\text{m}}08.4^{\text{s}}$, $\text{Dec} = +01^{\circ}00'38.8''$, J2000. The mapping grid spacing was $20''$ and the integration time was 20 s in each pointing. All the observations were performed in position-switching mode.

We used the XF digital spectrometer with the bandwidth and spectral resolution set to 128 MHz and 125 kHz. The velocity resolution was 0.11 km s^{-1} , the half-power beamwidth (HPBW) $22''$. The system temperature varied from $T_{\text{sys}} = 150$ to 300 K .

The main-beam efficiency was $\eta_{\text{mb}} \sim 0.65$. The spectra were Hanning smoothed to improve the signal-to-noise ratio, and only linear or some second-order polynomials were used for baseline fitting. The data were reduced with NEWSTAR¹ and the spectra processed using the XSpec software package².

Additionally, we used public $^{13}\text{CO } J = 1-0$ data, with an angular and spectral resolution of $46''$ and 0.2 km s^{-1} , obtained from the Galactic Ring Survey (GRS; Jackson et al. 2006), and near-IR UKIDSS data (Lucas et al. 2008) extracted from the WFCAM Science Archive³.

3. Results and discussion

Figure 1 displays the $^{12}\text{CO } J = 3-2$ spectra obtained towards the surveyed region. The centre, that is, the (0, 0) offset, corresponds to the position of MSXG34. The spectra present a main component with an absorption dip associated with MSXG34, and additionally less intense components at higher velocities, which appear in the whole surveyed area and represent gas detected along the line of sight not related to the analysed source. The same region was also surveyed in the $\text{HCO}^+ J = 4-3$ line, but emission was only detected at the (0, 0) offset. Figure 2 shows the ^{12}CO and HCO^+ spectra towards the centre of the region. The $^{12}\text{CO } J = 3-2$ spectrum shows a double-peak structure with a main component centred at $\sim 14.3 \text{ km s}^{-1}$ and a less intense component centred at $\sim 10.0 \text{ km s}^{-1}$. Both components are far to be Gaussian, and it is very likely that the line appears self-absorbed, as is commonly found towards star-forming regions (e.g. Johnstone et al. 2003; Buckle et al. 2010), which in this case is indicated by the absorption dip at $\sim 13.2 \text{ km s}^{-1}$. Moreover, the velocity of this absorption dip is almost coincident with those of the NH_3 lines detected by Wienen et al. (2012) ($v_{\text{LSR}} = 13.63$ and 13.85 km s^{-1} with $\Delta v_{\text{FWHM}} = 0.87$ and 1.13 km s^{-1} for $(J, K) = (1, 1)$ and $(2, 2)$ NH_3 inversion lines). The presence of ammonia, tracer of high density gas, confirms the density gradient that produces the self-absorption in the optically thick ^{12}CO line. On the other side, the HCO^+ spectrum shows a simpler behaviour and can be fitted with a Gaussian centred at $v_{\text{LSR}} \sim 14.2 \text{ km s}^{-1}$ with $\Delta v_{\text{FWHM}} \sim 1.6 \text{ km s}^{-1}$.

It is known that HCO^+ and NH_3 enhance in molecular outflows as reported by Torrelles et al. (1992), Girart et al. (1998), and Rawlings et al. (2004). In effect, an enhancement in the abundance of such molecular species is expected to occur in the boundary layer between the outflow and the surrounding molecular core. As these authors point out, this enhancement is probably due to the liberation and photoprocessing by the shock of the molecular material stored in the icy mantles of the dust. This process may be occurring in MSXG34, which is supported by the observed complexity in the $^{12}\text{CO } J = 3-2$ profiles that, as shown in Figs. 1 and 2, present spectral wings as usually observed towards molecular outflows.

Taking into account that $^{12}\text{CO } J = 3-2$ appears to be self-absorbed, a single-Gaussian function is expected to contain the two main components that are separated by the absorption dip. The emission that appears to be beyond the Gaussian shape is considered to be associated with the molecular outflows. This is shown in Fig. 3, where we display above the central ^{12}CO spectrum the Gaussian function and high-velocity gas intervals along

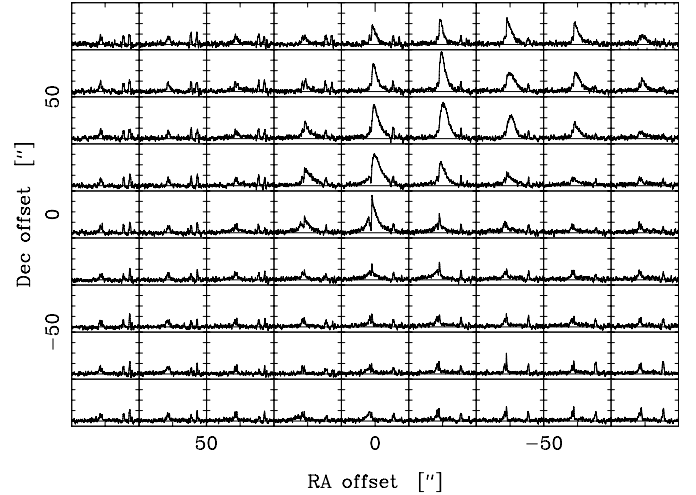


Fig. 1. $^{12}\text{CO } J = 3-2$ spectra obtained towards the surveyed region. The (0, 0) offset is the position of the studied source.

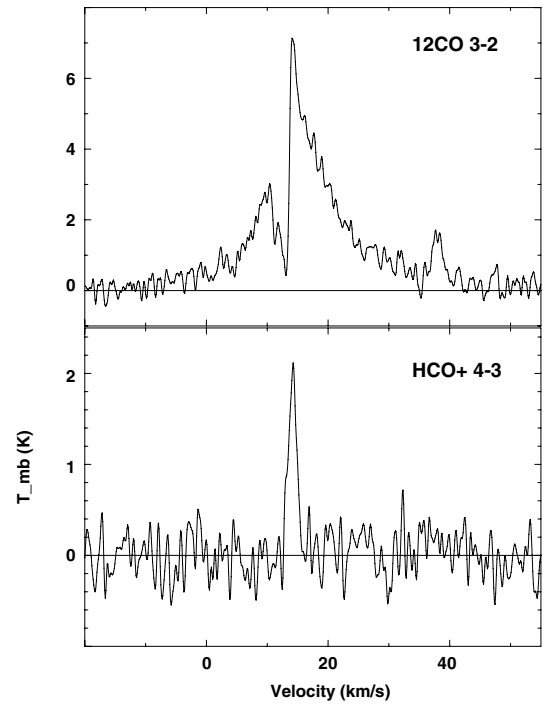


Fig. 2. $^{12}\text{CO } J = 3-2$ and $\text{HCO}^+ J = 4-3$ spectra obtained towards the centre of the surveyed region.

which the emission was integrated. The small component at $\sim 38 \text{ km s}^{-1}$ is excluded because, as shown in Fig. 1, it appears almost in the whole surveyed region, which precludes that it is produced by MSXG34. The result of the integration is shown in Fig. 4, where we display above the *Spitzer*-IRAC IR emission at $8 \mu\text{m}$ the $^{12}\text{CO } J = 3-2$ integrated between 20 and 35 km s^{-1} (red-shifted gas), and between -10 and 7 km s^{-1} (blue-shifted gas). An intense red-shifted ^{12}CO lobe clearly extends towards the north-west, while a less intense ^{12}CO blue-shifted lobe extends towards the south-west. Both lobes appear to be highly misaligned.

To roughly estimate the outflow mass, following Bertsch et al. (1993), we calculated the H_2 column density from

$$N(\text{H}_2) = 2.0 \times 10^{20} \frac{W(^{12}\text{CO})}{[\text{K km s}^{-1}]} (\text{cm}^{-2}),$$

¹ Reduction software based on AIPS developed at NRAO, extended to treat single dish data with a graphical user interface (GUI).

² XSpec is a spectral-line reduction package for astronomy that has been developed by Per Bergman at Onsala Space Observatory.

³ <http://surveys.roe.ac.uk/wsa/>

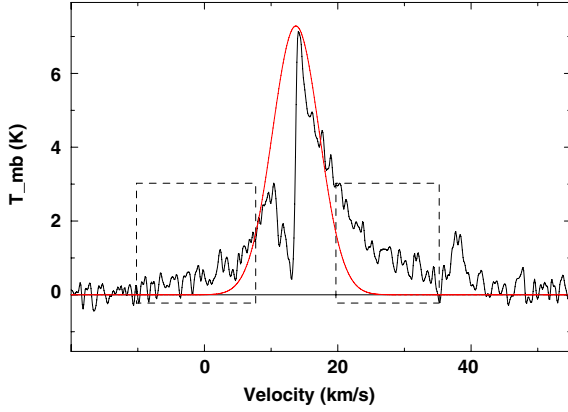


Fig. 3. $^{12}\text{CO } J = 3-2$ spectrum towards the centre of the surveyed region with a Gaussian function representing the unabsorbed main component. The boxes show the high-velocity gas intervals along which the emission was integrated.

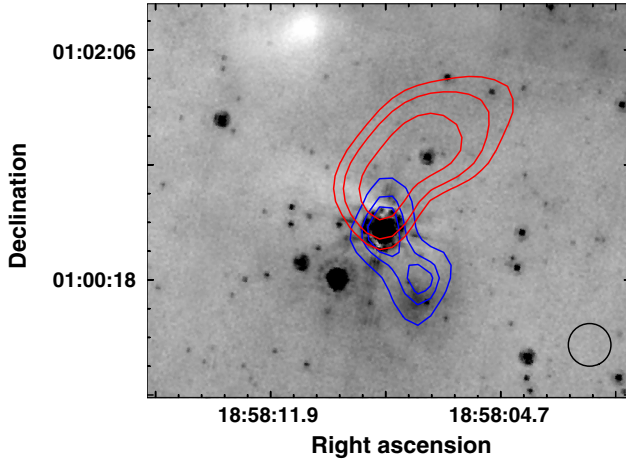


Fig. 4. *Spitzer*-IRAC $8 \mu\text{m}$ emission with contours of the $^{12}\text{CO } J = 3-2$ integrated between 20 and 35 km s^{-1} (in red), and between -10 and 7 km s^{-1} (in blue). The contour levels are 13, 17, and 25 K km s^{-1} for the red-shifted lobe, and 6.5, 7.5, and 8 K km s^{-1} for the blue-shifted one. The beam of the molecular observations is included in the bottom-right corner.

where $W(^{12}\text{CO})$ is the $^{12}\text{CO } J = 3-2$ integrated intensity along the velocity intervals shown in Fig. 2 (top). Then, the mass was derived from

$$M = \mu m_{\text{H}} \sum_i [D^2 \Omega_i N_i(\text{H}_2)],$$

where Ω is the solid angle subtended by the beam size, m_{H} is the hydrogen mass, μ , the mean molecular weight, is assumed to be 2.8 by taking into account a relative helium abundance of 25%, and D is the distance. We summed over all beam positions belonging to the lobes shown in Fig. 4, which yields the mass for the red- and blue-shifted outflows: $M_{\text{red}} \sim 7.5 M_{\odot}$ and $M_{\text{blue}} \sim 1.3 M_{\odot}$. Then we obtain the momentum $P_{\text{red}} \sim 114 \times \cos^{-1}(\phi) M_{\odot} \text{ km s}^{-1}$ and $P_{\text{blue}} \sim 22.5 \times \cos^{-1}(\phi) M_{\odot} \text{ km s}^{-1}$, and the energies $E_{\text{red}} \sim 3.4 \times 10^{46} \times \cos^{-2}(\phi) \text{ erg}$ and $E_{\text{blue}} \sim 7.6 \times 10^{45} \times \cos^{-2}(\phi) \text{ erg}$, where ϕ is the inclination angle of the outflow, which is uncertain.

3.1. Outflows morphology

As mentioned above and shown in Fig. 4, the red- and blue-molecular outflows are highly misaligned. A jet precession,

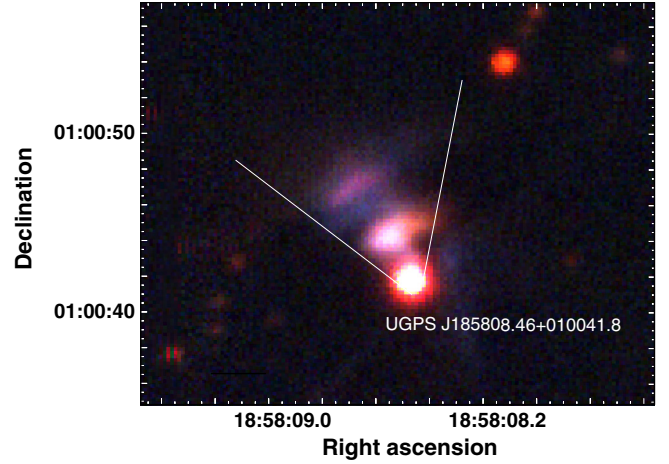


Fig. 5. Three-colour image towards MSXG34 where the *JHK*-bands from UKIDSS are presented in blue, green, and red. The angular resolution is about 1 arcsec.

either produced by tidal interactions in a binary system or due to anisotropic accretion events (e.g. Papaloizou & Terquem 1995; Kraus et al. 2006), can generate misaligned molecular outflows. We found a similar case as presented here towards the UCHII region G045.47+0.05 (Ortega et al. 2012). Two misaligned red- and blue-shifted molecular outflows were discovered through molecular observations obtained with ASTE. Later, from very high-angular resolution observations at near-IR obtained with Gemini-NIRI, Paron et al. (2013) reported that a jet precession occurs in a massive YSO. Another similar case in which a jet precession scenario was suggested is IRAS 20126+4104, where two misaligned CO high-velocity flows are observed (Lebrón et al. 2006). To investigate this possibility we analysed near-IR data from UKIDSS towards MSXG34.

Figure 5 shows the emission of the *JHK*-bands from UKIDSS in a three-colour image. The point source UGPS J185808.46+010041.8 (Lucas et al. 2008; Ukidss 2012) is connected with a cone-like nebulosity composed of two arc-like features, the closest feature more intense than the farther. Both features seem to be connected by diffuse emission. It is very likely that the near-IR emission forming this cone-like shape arises from a cavity cleared in the circumstellar material. This emission can be due to a combination of different emitting processes: continuum emission from the central protostar that is scattered at the inner walls of a cavity, emission from warm dust, and probably also emission lines from shock-excited gas. The arc-like features, with a concavity pointing to the source, suggest an spiraling shape, which can be signature of a precessing jet. This can be a similar case as we found in G045.47+0.05 (Paron et al. 2013) and others in the literature (e.g. Weigelt et al. 2006; Kraus et al. 2006). Therefore, we conclude that the misaligned CO outflows and the near-IR features related to the analysed source strongly suggest a jet-precession scenario. However, higher angular resolution observations in both submillimeter and near-IR are necessary to investigate the whole circumstellar region in more detail.

Additionally, analysing the molecular gas on a larger scale, we found that MSXG34 lies in a molecular clump. Thus, a complementary possible scenario for the misaligned molecular outflows is that one of its lobes is deflected by the interaction with dense material. By inspecting the $^{13}\text{CO } J = 1-0$ cube obtained from the GRS, we found that the molecular clump in which MSXG34 is likely embedded extends from 10 to 14 km s^{-1} . Taking into account that the systemic velocity of MSXG34 is

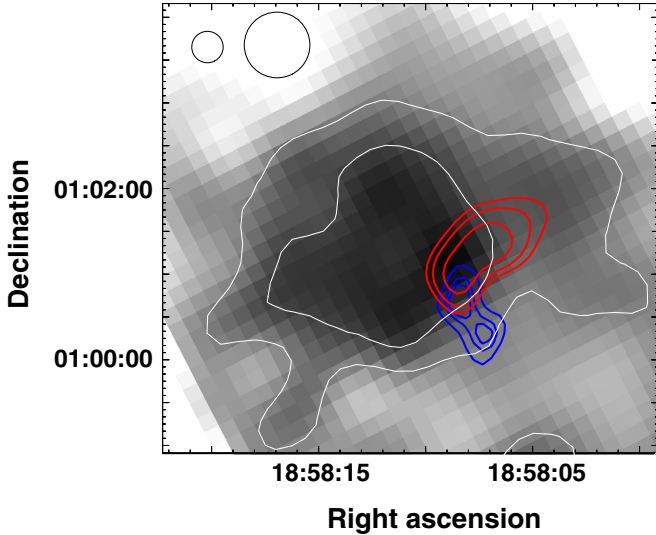


Fig. 6. $^{13}\text{CO } J = 1-0$ obtained from the GRS integrated between 10 and 14 km s^{-1} . The contour levels are 6.8 and 7.5 K km s^{-1} . The contours of the blue and red lobes shown in Fig. 4 are also displayed. The ASTE and GRS beams are included in the top-left corner.

about 14 km s^{-1} (determined from the emission of NH_3 and HCO^+), the formation of this YSO would be occurring at the far border of the clump. Figure 6 shows the $^{13}\text{CO } J = 1-0$ emission integrated between 10 and 14 km s^{-1} with contours of the blue- and red-shifted molecular outflows. The scenario might be that the YSO is located in the background border of the molecular clump, the red-shifted lobe freely flows away, while the blue-shifted one hits the inner and densest portion of the clump which deflects its trajectory. It might be a similar case as discovered in the NGC 1333 IRAS 4A region by Choi (2005). Submillimeter observations of high-density tracers such as CS and SiO, are necessary to confirm the existence of high-density gas belonging to the clump and to study the probable collision with the blue lobe. Finally, another possibility is that the red- and blue-shifted lobes come from monopolar molecular outflows, as proposed by Fernández-López et al. (2013) in IRAS 18162-2048, where the respective counterlobes are not seen because they are passing through a cavity and/or regions of low molecular abundance.

3.2. Nature of the outflow-driving source

The analysis of the UKIDSS data suggests that source UGPS J185808.46+10041.8 is a good candidate to be the driving source of the discovered molecular outflow (see Fig. 7). This near-IR source is embedded in a clump of cold dust catalogued as G034.60-1.030 in the ATLASGAL cold high-mass clumps with NH_3 catalogue (Wienen et al. 2012). By considering the associated dust continuum emission at $870 \mu\text{m}$ and following Beuther et al. (2005) and Hildebrand (1983), we estimate the mass of this clump from

$$M_{\text{gas}} = \frac{2.0 \times 10^{-2}}{J_{\nu}(T_{\text{dust}})} \frac{a}{0.1 \mu\text{m}} \frac{\rho}{3 \text{ g cm}^{-3}} \frac{R}{100 \text{ Jy}} \frac{F_{\nu}}{\left(\frac{d}{\text{kpc}}\right)^2} \times \left(\frac{\nu}{1.2 \text{ THz}}\right)^{-3-\beta}, \quad (1)$$

where $J_{\nu}(T_{\text{dust}}) = [\exp(h\nu/kT_{\text{dust}}) - 1]^{-1}$ and a, ρ, R , and β are the grain size, grain mass density, gas-to-dust ratio, and grain emissivity index, for which we adopt the values of $0.1 \mu\text{m}$, 3 g cm^{-3} ,

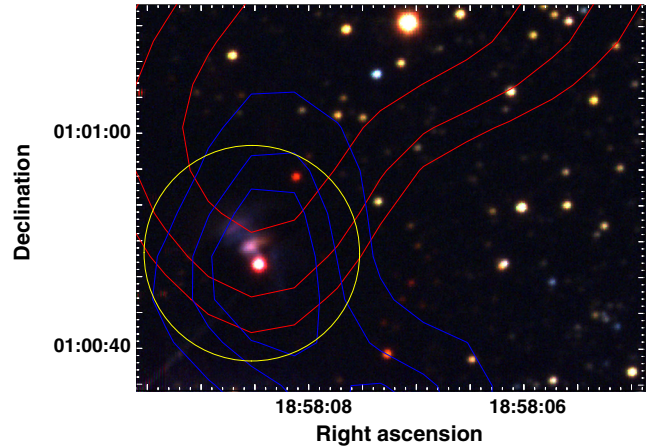


Fig. 7. UKIDSS three-colour image (JHK -bands in blue, green and red) of the MSXG34 region. The red- and blue-shifted lobes of the molecular outflows are included. The yellow circle, $30''$ in size, corresponds to the $500 \mu\text{m}$ continuum emission from SPIRE (above 5σ of the rms noise level) as extracted from the *Herschel* Science Archive.

100, and 2, respectively (Hunter 1997, Hunter et al. 2000, and Molinari et al. 2000). Assuming a dust temperature of 20 K and considering the integrated flux intensity $F_{\nu} = 1.8 \text{ Jy}$ at $870 \mu\text{m}$ (Wienen et al. 2012), we obtain $M_{\text{gas}} \sim 25 M_{\odot}$. On the other hand, considering the integrated flux density $F_{\nu} = 19.2 \text{ Jy}$ at $500 \mu\text{m}$ obtained from the level-2 PLW *Herschel* image using the HIPE software package (Ott 2010), and using the above equation with the same considerations, we estimate a mass for the clump of about $40 M_{\odot}$. Thus, we conclude that UGPS J185808.46+10041.8 is embedded in a high-mass clump (around $30 M_{\odot}$).

To better characterize the nature of this IR source, we fitted the spectral energy distribution (SED) using the online tool developed by Robitaille et al. (2007)⁴. We adopted an interstellar extinction on the line of sight, A_{ν} , between 1 and 50 mag. We assumed a 20% uncertainty for the distance to UGPS J185808.46+10041.8. In Fig. 8 we show the SED with the best-fitting model (black curve), and the subsequent well-fitting models (gray curves) with $\chi^2 - \chi^2_{\text{best}} \leq 3$ (where χ^2_{best} is the χ^2 per data point of the best-fitting model for the source). To construct this SED we used fluxes extracted from the UKIDSS-DR6 Galactic Plane Survey (Lucas et al. 2008) in the J , H and K bands (source UGPS J185808.46+010041.8), the MSX Point Source Catalog at 8.2 , 12.1 , 14.6 , and $21.3 \mu\text{m}$ (source G034.5964-01.0292), the WISE All-Sky Source Catalog⁵ at 3.6 , 12 , and $22 \mu\text{m}$ (source WISE J185808.44+010041.8), the PACS bands at 70 and $160 \mu\text{m}$ (Poglitsch et al. 2010), the SPIRE bands at 250 , 350 , and $500 \mu\text{m}$ (Griffin et al. 2010) from *Herschel*, and finally ATLASGAL at $870 \mu\text{m}$. PACS and SPIRE fluxes were obtained from level-2 MADmaps, PLW, PMW, and PSW images, respectively, using HIPE software package. Considering that UGPS J185808.46+010041.8 is by far the brightest source within the *Herschel* emission boundaries (see yellow circle in Fig. 7) and no contamination from clustering of infrared objects is observed in the region, we treated the larger beam-size data of WISE at $22 \mu\text{m}$, *Herschel*, and ATLASGAL as “data points” instead of upper limits to make the best use of all data in constraining the

⁴ <http://caravan.astro.wisc.edu/protostars/>

⁵ WISE is a joint project of the University of California, Los Angeles, and the Jet Propulsion Laboratory/California Institute of Technology, funded by NASA.

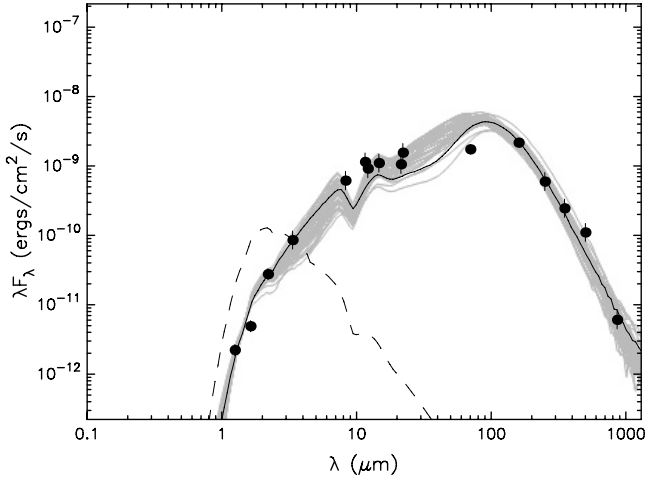


Fig. 8. SED of MSXG34. The circles indicate the measured fluxes of the data points. The black and grey solid curves represent the best-fitting model and the subsequent well-fitting models (with $\chi^2 - \chi^2_{\text{best}} \leq 3$), respectively. The dashed line shows the stellar photosphere corresponding to the central source of the best-fitting model, as it would look without circumstellar dust.

Table 1. Main physical parameters from the SED of MSXG34.

M_\star [M_\odot]		Age [$\times 10^4$ yr]		\dot{M}_{env} [$\times 10^{-4} M_\odot \text{ yr}^{-1}$]		L [$\times 10^2 L_\odot$]	
Mean	Range	Mean	Range	Mean	Range	Mean	Range
3	1.5–8	1.0	0.1–3	6	1–10	1.9	0.5–5

SED. 20% errors on the fluxes were assumed for all data, except for UKIDSS fluxes, where 30% error were used because of extinction uncertainties.

The SED was fitted by multiple models, each model describing a set of physical parameters. The same parameter from different models can have a wide range, spanning from several factors to orders of magnitudes. We obtained 63 well-fitting models that satisfy the χ^2 criterion mentioned above. To find a representative value for the distributions of the parameters, we computed a weighted mean and a range of values for some of the physical parameters of the source (see Table 1). The weight used for the weighted means is the inverse of the χ^2 of each model. It is important to mention that the trend of our fitting results are not biased by the trend inherent in the model grids. The SED analysis of UGPS J185808.46+010041.8 suggests that the central object is a young intermediate-mass protostar of about $3 M_\odot$. By comparing the obtained bolometric luminosity of about $200 L_\odot$ with the total outflow mass, about $9 M_\odot$, we note that it agrees well, within the dispersion, with the relation found by Wu et al. (2004). The position of our point in the figure presented by the authors displaying M_{out} vs. L_{bol} also suggests an intermediate-mass protostar.

4. Summary

Using the ASTE telescope, we observed MSXG34, a catalogued massive YSO at a distance of about 1 kpc, in the $^{12}\text{CO } J = 3-2$ and $\text{HCO}^+ J = 4-3$ lines with the aim of discovering and studying molecular outflows. The ^{12}CO spectra towards the YSO present typical signatures of star-forming regions: a self-absorption dip and spectral wings that indicate outflow activity. The HCO^+ was detected only towards the MSXG34 position

at $v_{\text{LSR}} \sim 14.2 \text{ km s}^{-1}$, in coincidence with the ^{12}CO absorption dip and approximately with the velocity of previous ammonia observations. The HCO^+ and NH_3 are known to be enhanced in molecular outflows.

By analysing the $^{12}\text{CO } J = 3-2$ emission, we discovered misaligned red- and blue-shifted molecular outflows with mass, momentum, and energy of $M_{\text{red}} \sim 7.5 M_\odot$ and $M_{\text{blue}} \sim 1.3 M_\odot$, $P_{\text{red}} \sim 114 \times \cos^{-1}(\phi) M_\odot \text{ km s}^{-1}$ and $P_{\text{blue}} \sim 22.5 \times \cos^{-1}(\phi) M_\odot \text{ km s}^{-1}$, and $E_{\text{red}} \sim 3.4 \times 10^{46} \times \cos^{-2}(\phi) \text{ erg}$ and $E_{\text{blue}} \sim 7.6 \times 10^{45} \times \cos^{-2}(\phi) \text{ erg}$, where ϕ is the inclination angle of the outflow, which is uncertain.

By analysing UKIDSS near-IR data, we found that the emission shows a cone-like nebosity composed of two arc-like features related to the YSO, which can be due to a cavity cleared in the circumstellar material by a precessing jet, explaining in this way the misalignment in the molecular outflows. Additionally, the $^{13}\text{CO } J = 1-0$ data show that MSXG34 is very likely embedded in a molecular clump that extends from 10 to 14 km s^{-1} . Taking into account that the associated central velocity of MSXG34 is about 14 km s^{-1} , it is probable that the YSO is located in the background of the densest part of the clump, and thus the blue-shifted outflow is probably deflected by the interaction with dense gas along the line of sight. Another possibility is that the red- and blue-shifted lobes come from monopolar molecular outflows, where the respective counterlobes are not seen because they are passing through a cavity and/or regions of low molecular abundance.

Finally, we performed an SED analysis using fluxes from near- to far-IR that suggested that the central object of MSXG34 is a young intermediate-mass protostar (about $3 M_\odot$). The relation between the total outflow mass, obtained from our molecular observations, and the bolometric luminosity, obtained from the SED, also suggests an intermediate-mass stellar object.

Acknowledgements. We would like to thank the anonymous referee for her/his helpful comments. S.P. and M.O. are members of the *Carrera del investigador científico* of CONICET, Argentina. A.P. is a post-doctoral fellow of CONICET, Argentina. This work was partially supported by grants awarded by CONICET, ANPCYT, and UBA (UBACyT). M.R. wishes to acknowledge support from FONDECYT(CHILE) grant No1140839. A.P. is very grateful to the ASTE staff for the support received during the observations. The ASTE project is driven by Nobeyama Radio Observatory (NRO), a branch of the National Astronomical Observatory of Japan (NAOJ), in collaboration with University of Chile, and Japanese institutes including the University of Tokyo, Nagoya University, Osaka Prefecture University, Ibaraki University, Hokkaido University, and Joetsu University of Education.

References

- Arce, H. G., Borkin, M. A., Goodman, A. A., Pineda, J. E., & Halle, M. W. 2010, *ApJ*, 715, 1170
- Baek, C. H., Kim, J., & Choi, M. 2009, *ApJ*, 690, 944
- Bally, J., Licht, D., Smith, N., & Walawender, J. 2006, *AJ*, 131, 473
- Bertsch, D. L., Dame, T. M., Fichtel, C. E., et al. 1993, *ApJ*, 416, 587
- Beuther, H., Schilke, P., Menten, K. M., et al. 2005, *ApJ*, 633, 535
- Buckle, J. V., Curtis, E. I., Roberts, J. F., & et al. 2010, *MNRAS*, 401, 204
- Choi, M. 2005, *ApJ*, 630, 976
- Cunningham, N. J., Moeckel, N., & Bally, J. 2009, *ApJ*, 692, 943
- Ezawa, H., Kawabe, R., Kohno, K., & Yamamoto, S. 2004, in *SPIE Conf. Ser.* 5489, ed. J. M. Oschmann, Jr., 763
- Fernández-López, M., Girart, J. M., Curiel, S., et al. 2013, *ApJ*, 778, 72
- Fich, M., & Lada, C. J. 1997, *ApJ*, 484, L63
- Froebrich, D., Smith, M. D., & Eislöffel, J. 2003a, *Ap&SS*, 287, 217
- Froebrich, D., Smith, M. D., Hodapp, K.-W., & Eislöffel, J. 2003b, *MNRAS*, 346, 163
- Girart, J., Estalella, R., & Ho, P. T. P. 1998, *ApJ*, 495, L59
- Griffin, M. J., Abergel, A., Abreu, A., et al. 2010, *A&A*, 518, L3
- Hildebrand, R. H. 1983, *QJRAS*, 24, 267

- Hunter, T. R. 1997, Ph.D. Thesis, Smithsonian Astrophysical Observatory, Cambridge, USA
- Hunter, T. R., Churchwell, E., Watson, C., et al. 2000, *AJ*, 119, 2711
- Jackson, J. M., Rathborne, J. M., Shah, R. Y., et al. 2006, *ApJS*, 163, 145
- Johnstone, D., Boonman, A. M. S., & van Dishoeck, E. F. 2003, *A&A*, 412, 157
- Kraus, S., Balega, Y., Elitzur, M., et al. 2006, *A&A*, 455, 521
- Kuchar, T. A., & Clark, F. O. 1997, *ApJ*, 488, 224
- Lebrón, M., Beuther, H., Schilke, P., & Stanke, T. 2006, *A&A*, 448, 1037
- Lockman, F. J. 1989, *ApJS*, 71, 469
- Lucas, P. W., Hoare, M. G., Longmore, A., et al. 2008, *MNRAS*, 391, 136
- Lumsden, S. L., Hoare, M. G., Urquhart, J. S., et al. 2013, *ApJS*, 208, 11
- Molinari, S., Brand, J., Cesaroni, R., & Palla, F. 2000, *A&A*, 355, 617
- Ortega, M. E., Paron, S., Cichowolski, S., Rubio, M., & Dubner, G. 2012, *A&A*, 546, A96
- Ott, S. 2010, in *Astronomical Data Analysis Software and Systems XIX*, eds. Y. Mizumoto, K.-I. Morita, & M. Ohishi, *ASP Conf. Ser.*, 434, 139
- Papaloizou, J. C. B., & Terquem, C. 1995, *MNRAS*, 274, 987
- Paron, S., Fariña, C., & Ortega, M. E. 2013, *A&A*, 559, L2
- Poglitsch, A., Waelkens, C., Geis, N., et al. 2010, *A&A*, 518, L2
- Rawlings, J. M. C., Redman, M. P., Keto, E., & Williams, D. A. 2004, *MNRAS*, 351, 1054
- Robitaille, T. P., Whitney, B. A., Indebetouw, R., & Wood, K. 2007, *ApJS*, 169, 328
- Torrelles, J. M., Rodríguez, L. F., Canto, J., et al. 1992, *ApJ*, 396, L95
- Ukidss, C. 2012, *VizieR Online Data Catalog: II/316*
- Weigelt, G., Beuther, H., Hofmann, K.-H., et al. 2006, *A&A*, 447, 655
- Wienen, M., Wyrowski, F., Schuller, F., et al. 2012, *A&A*, 544, A146
- Wu, Y., Wei, Y., Zhao, M., et al. 2004, *A&A*, 426, 503